Comparative binding pattern analysis of 5-MeO-DMT and 7-MeO-DMT against 5HT2A receptor employing molecular docking, MMGB-SA and molecular dynamics studies.

Rishabh Khare[a], Kalirajan Rajgopal[b*], Kaveri prasad[c], Srikanth Jupudi[d], Preeya Negi[e], Jayanthi Koppula[f]

Keywords: 5-MeO-DMT, 7-MeO-DMT, Antidepressant, Psychedelics, 5HT2AR.

Abstract

Depression calls for attention since it affects around 5% of the world's population and investigators are encouraged to develop effective antidepressants. According to the monoamine-deficiency hypothesis, the underlying pathophysiology of depression is that it occurs when the brain lacks certain neurotransmitters (such as serotonin, norepinephrine, or dopamine). The neurotransmitter serotonin has received the greatest attention in relation to depression. According to studies, 5-MeO-DMT (5-methoxy-N, N-dimethyltryptamine) elevates intersynaptic serotonin levels when administered as a single inhalation of vapour from dried toad secretion and produces higher life satisfaction, convergent thinking, higher ratings of mindfulness, and lower ratings of depression and anxiety. It also lowers biomarkers of stress such as cortisol. But 5-MeO-DMT is a psychedelic that has hallucinogenic effects, so a comparative study between 5-MeO-DMT and its non-hallucinogenic analogue 7-MeO-DMT (7-methoxy-N, N-dimethyltryptamine) is performed in order to compare its binding affinity, stability of ligand within the active site through computational studies. In order to determine whether 7-MeO-DMT can be a potential candidate as an anti-depressant. 5-MeO-DMT and 7-MeO-DMT were sketched using Marvin and molecular docking studies were performed using XP (extra precision) docking in order to evaluate the binding interaction accomplished by protein-ligand complex. The Gilde XP docking data indicated the GScores of 5-MeO-DMT (-8.01kcal/mol) and 7-MeO-DMT (-7.92kcal/mol), furthermore MM-GBSA indicated a binding free energy (ΔBind) of -51.68 and 73.25 kcal/mol respectively where 7-MeO-DMT performed better than that of 5-MeO-DMT. Calculations were also made for other ligand characteristics such radius gyration, molecular surface area, solvent accessible surface area, and polar surface area.

* Corresponding Authors
E-Mail: rkalirajan@jssuni.edu.in

[a] Department of Pharmaceutical Chemistry, JSS College of Pharmacy, JSS Academy of Higher Education & Research, Ooty, Nilgiris, Tamil Nadu, India; rishabhkhare2121@gmailcom

[b] Department of Pharmaceutical Chemistry, JSS College of Pharmacy, JSS Academy of Higher Education & Research, Ooty, Nilgiris, Tamil Nadu, India: kaveriprasadmpm@gmail.com

[c] Department of Pharmaceutical Chemistry, JSS College of Pharmacy, JSS Academy of Higher Education & Research, Ooty, Nilgiris, Tamil Nadu, India; rkalirajan@jssuni.edu.in

[d] Department of Pharmaceutical Chemistry, JSS College of Pharmacy, JSS Academy of Higher Education & Research, Ooty, Nilgiris, Tamil Nadu, India; sjphd@jssuni.edu.in

[e] Department of Pharmaceutical Chemistry, JSS College of Pharmacy, JSS Academy of Higher Education & Research, Ooty, Nilgiris, Tamil Nadu, India; negipreeya1@gmail.com

[f] Department of Pharmaceutical Chemistry, JSS College of Pharmacy, JSS Academy of Higher Education & Research, Ooty, Nilgiris, Tamil Nadu, India; jayanthikopppula145@gmail.com

1. Introduction

Up to 40% of individuals with depression do not react adequately to antidepressant drugs, making depression one of the most serious mental diseases impacting millions of people worldwide (1,2). Depressive disorders, which are common, burdensome, and expensive, have been linked to considerable impairments in work roles and quality standards of living, as well as medical comorbidity and mortality (3). According to the monoamine hypothesis, one of the pathophysiological bases of depression is low levels of norepinephrine, serotonin and/or dopamine in the brain (4). Because most studies focus on the neurotransmitter serotonin, increasing its levels can help improve mood and relieve depressive symptoms (5). Central serotonin deficiency is linked to mood-related memory distortions, reward-related changes in behaviour, and interruption of inhibitory emotional processing (6,7). As a result, increasing inter-synaptic serotonin concentrations may help.

Psychedelics are significant for this research because they are powerful psychoactive compounds that may affect emotions and a wide range of cognitive functions (8). The psychedelic chemical family is called psychoplastogens (9). Psychedelics, in particular, are mentally safe, have few withdrawal symptoms, pose a low risk of addiction or dependency, and have no long-term physiological or psychological side effects (10). Furthermore, psychedelics have significantly fewer harmful side effects than traditional antidepressants. Psychedelics deliver therapeutic results in patients more quickly and may have beneficial, long-lasting benefits with only one pill or treatment session (11). Numerous plant and animal species (Colorado River toad) produces the short-acting psychedelic tryptamine 5-Methoxy-N,N-dimethyltryptamine (5-MeO-DMT). Historically, 5-MeO-DMT-containing plants have been utilized in religious and spiritual contexts (12,13). After administering the medication with one thorough inhalation of toad secretion vapour, researchers discovered reduced levels of depression, anxiety, and tension; increased levels of convergent thinking and life satisfaction; and enhanced mindfulness assessments (14,15). In a study, it was found that inhaling synthetic 5-MeO-DMT lowered stress biomarkers like cortisol (16). 5-MeO-DMT has been proven in studies to have antidepressant and anxiolytic properties, with no negative physical or psychological consequences and a low risk for addiction (10,15). However, one of the major disadvantages of 5-MeO-DMT is its ability to induce hallucinations: furthermore, structure-activity relationship studies revealed that simply shifting the methoxy group position from 5th to 7th can prevent the hallucinogenic effects in 7-MeO-DMT (7-methoxy-N,N-dimethyltryptamine) while retaining its therapeutic potential (17).

Psychedelics show their behavioural effects after their binding to 5-HT2AR (5-hydroxy-tryptamine 2A receptor) (18). Indolealkylamines (5-MeO-DMT and 7-MeO-DMT) have

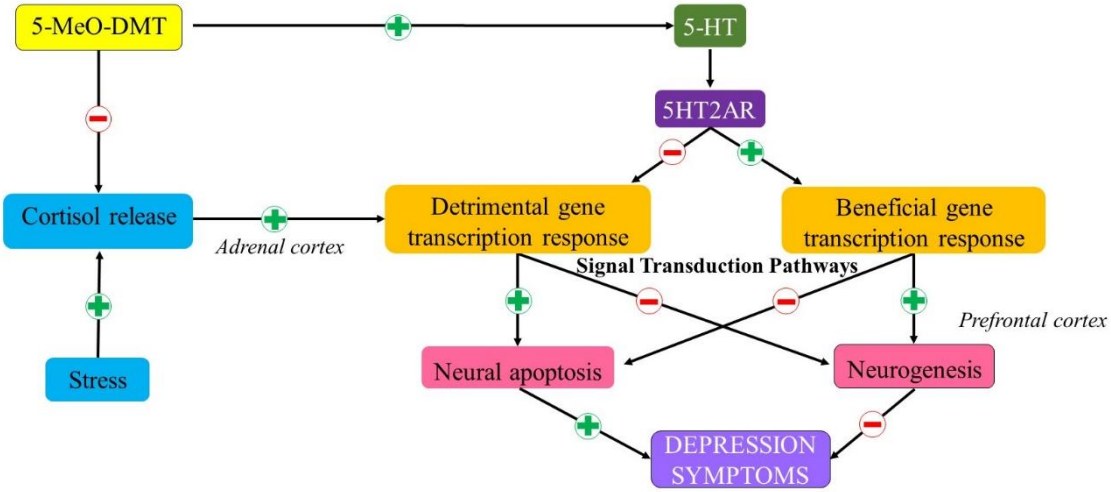

Figure 1. Pathway of 5-MeO-DMT activity in depression through 5HT2AR

agonistic interactions with the 5-HT2AR [Structure–Activity Relationships of phenylalkylamines as Agonist Ligands for 5-HT2A Receptors] (19). Serotonin 5-hydroxytryptamine 2A receptors (5-HT2ARs) are abundant in the brain and other portions of the central nervous system, particularly memory and thought-related regions. Several hallucinogens, antipsychotics, and antidepressants work by focusing on 5-HT2ARs in addition to endogenous 5-HT (20,21). Agonists of the 5-HT2A receptor are thought to have a long-lasting therapeutic impact on depressive disorders through increasing neuronal development in the brain's anterior structures, such as the prefrontal cortex **(Figure 1)** (22). As a result of the correlation between neural patterns and symptoms, modulating the plasticity of brain circuits may reverse pathogenic abnormalities within these structures, resulting in a longer-lasting therapeutic effect than simply alleviating the disorder's symptoms (23,24).

2. Materials and Methods

2.1. Molecular docking

Schrodinger's Suite 2020-1's Protein Preparation Wizard was used for the preparation of the 3D X-ray crystal structure of the serotonin 2A receptor-Gq protein co-crystallized with hallucinogenic ligand after it was downloaded from Protein Data Bank (6WGT.pdb) (25). 6WGT.pdb is a homotrimer that consists of chains A, B, and C. Chain C with co-crystalline hallucinogenic agonist defining the active site is preserved **(Figure 2)**, while the non-redundant chains were eliminated.

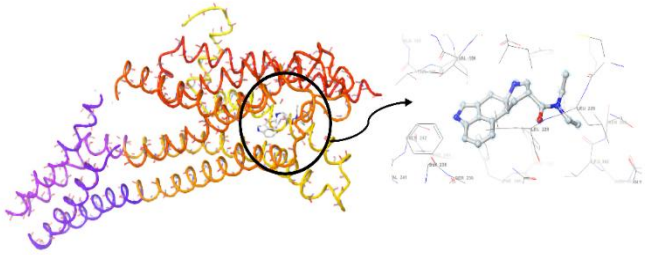

Figure 2. 5HT2AR with co-crystalline hallucinogenic agonist

The protein was prepared by removing crystal fluids and adjusting bond order with hydrogen additions, and the Epik module was used to complete the protonation and tautomeric states of acidic and basic residues at pH 7.2 by adding missing side chains and loops (26,27). OPLS3e (Optimized Potentials for Liquid Simulations) molecular force-field (28) is used to minimize the protein, with the crystallographic heavy atoms root mean square deviation (RMSD) set to 0.30Å. A grid box with its center at the active site's centroid (x=24.55; y=-36.95; z=54.83) was created using a van der Waals scale of 1.0 for the receptor and a partial charge cut-off of 0.25. Using Marvin, the structure of 5-MeO-DMT and 7-MeO-DMT was sketched (29). The binding site for the 5-HT2AR (6WGT.pdb) was used to start a virtual workflow in XP (Extra Precision) mode with their default settings. The prediction of the ligand's conformation and pose (its projected placement and orientation inside these sites) is the first step in docking, followed by an assessment of the binding affinity (30). Using the Glide Gscore, glide energy data, and hydrogen bond analysis, the optimal binding pose was determined.

2.2. ADME Study

The ADME (absorption, distribution, metabolism, and excretion) characteristics of compounds are one of the most critical requirements for a drug to be a viable candidate. Poor ADME qualities cause about 40% of drug candidates to fail in clinical studies. The in-silico ADME characteristics of 5-MeO-DMT and 7-MeO-DMT were found using the Schrodinger suite's QikProp module (31). Lipinski's rule is the most often used method for determining drug-likeness. Lipinski and colleagues at Pfizer developed the rule of five, which states that physicochemical parameters should fall within the following range: molecular weight < 500, logPo/w < 5, H- bond donor ≤ 5, and H- bond acceptor ≤10. Additionally, when two or more of the conditions are not met, a chemical is more likely to demonstrate poor absorption or poor permeation. QPPCaco forecasts the permeability model of Caco2 cells for the gut-blood barrier in the nonactive transport of human absorption process. Compounds with logBB greater than 0.3 pass the blood-brain barrier (BBB), but those with logBB greater than 1.0 are only poorly dispersed in the brain. The number of potential metabolic reactions is displayed by #metab, which should be between 1 and 8.

2.3. MM-GBSA free energy calculation studies

The prime MM-GBSA technique was applied to the generalized-born/surface area (GB/SA) continuum solvent

model to assess the relative importance of the enthalpy and entropy-associated components in the binding of the ligand-protein complex (32). The formula used to calculate the energy contributions from molecular mechanics, polar solvation, and a non-polar solvation factor (in kilocalories per mole) is:

$\Delta G_{bind} = G_{complex} - G_{protein} - G_{ligand}$

ΔG_{bind} = Calculated binding free energy (complex)

$G_{complex}$ = Binding free energy (minimized complex)

$G_{protein}$ = Binding free energy (receptor)

G_{ligand} = Binding free energy (unbound ligand)

2.4. Molecular dynamics (MD) simulation

To investigate the atomic-level binding behaviour of a highly rated molecule and to interpret the molecular interaction analysis, a molecular dynamics simulation was run utilizing the Desmond module of Schrodinger 2020-1, LLC, New York, NY (33). TIP3P water model was used for solvation of the complex of 5-MeO-DMT/6WGT and 7-MeO-DMT/6WGT in an orthorhombic periodic boundary condition with a 20Å buffer zone between the protein atoms and box borders. The addition of 0.15M NaCl counter ions aided in neutralizing the solvated system. Following that, the energy of the system was minimized using the OPLS3e force field (28). The long-range electrostatic interactions were computed with a 1e-09 tolerance using the smooth particle mesh Ewald technique. The van der Waals and coulomb interactions in the short-range were estimated at a cut-off radius of 0.9. A simulation lasting 100ns was run under an isothermal/isobaric ensemble at 300K and 1 bar of pressure (NPT). The Nose-Hoover chain thermostat (34) and Martyna-Tobias-Klein barostat (35) approaches were combined at 100 and 200 ps, respectively. Several time-step algorithms RESPA (Reference System Propagator Algorithm) were used at 2, 2, and 6 fs for bonded, short-range non-bonded, and long-range electrostatic forces. The data was collected every 100ps interval and the generated trajectories were examined.

3. Results and Discussion

3.1. Molecular Docking and MM-GBSA free energy calculation

5-MeO-DMT and 7-MeO-DMT were drawn in Marvin and ligand preparation was done using the Schrodinger suit. XP (extra precision) docking was done using default parameters. After XP docking, the binding poses and hydrogen bond formation for the two ligands (5-MeO-DMT, 7-MeO-DMT) were visually examined. The Prime module MM-GBSA was used for post-docking minimization. Tables 1 and 2 respectively tabulate the glide score and the prime MM-GBSA energy values.

Table 1. Glide XP docking values (kcal/mol) for 5-MeO-DMT and 7-MeO-DMT in the active site of 5HT2AR (6WGT.pdb).

S. No.	Compound	Glide GScore	Glide eVdW	Glide ECoul	Glide energy	Glide emodel
1	5-Meo-DMT	-8.01	-28.56	-4.02	-32.58	-43.43
2	7-Meo-DMT	-7.92	-24.63	-4.68	-29.31	-38.09

Table 2. Prime MMGB-SA binding free energy values (kcal/mol) for 5-MeO-DMT and 7-MeO-DMT in the active site of 5HT2AR (6WGT.pdb).

S. No.	Compound	dG_Bind	dG_Bind Coulomb	dG_Bind Covalent	dG_Bind Hbond	dG_Bind Lipo	dG_Bind VdW
1	5-Meo-DMT	-51.68	-18.61	-8.93	-5.39	-13.76	-3.74
2	7-Meo-DMT	-73.25	-48.73	-63.09	-7.38	-3.82	2.16

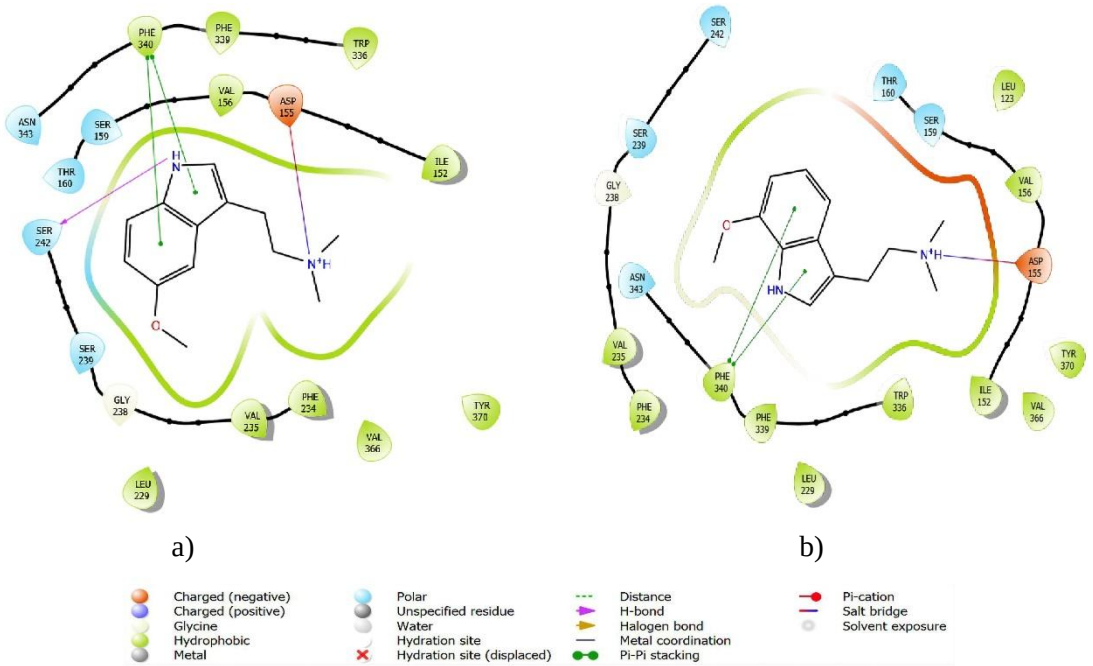

Figure 3. 2D interaction diagrams of (a) 5-MeO-DMT and (b) 7-MeO-DMT in the active site of 5-HT2AR (6WGT.pdb).

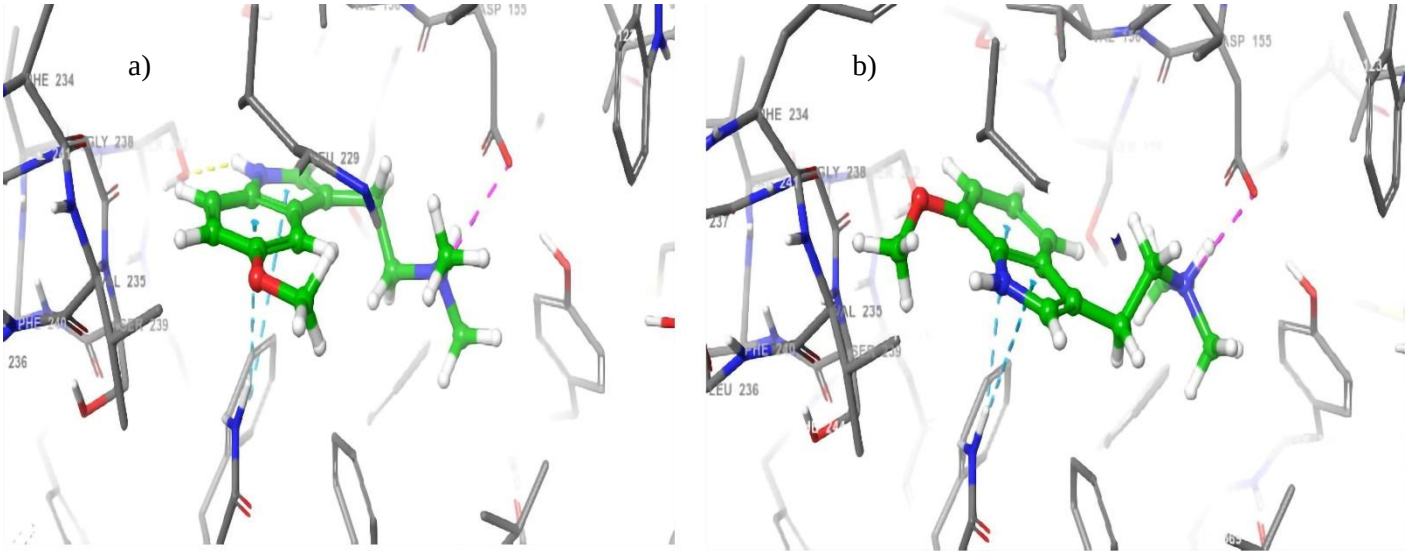

Figure 4. 3D interaction diagrams of (a) 5-MeO-DMT and (b) 7-MeO-DMT in the active site of 5-HT2AR (6WGT.pdb)

Figure 3 and Figure 4 depicts the 2D interactions and 3D interactions diagrams of 2-hits, 5-MeO-DMT and 7-MeO-DMT respectively, and hydrogen bonding, hydrophobic interaction, salt bridge and pi-pi stacking were mainly observed in the XP docked poses of 5-MeO-DMT and 7-MeO-DMT, predominantly with binding site residues, Ile152, Ash155, Val156, Ile210, Leu229, Phe234, Val235, Trp336, Phe339, Phe340, Asn343, Val366, Tyr370. The Glide GScores of 5-MeO-DMT and 7-MeO-DMT were predicted to be -8.01 and -7.92 kcal/mol, respectively.

The molecule 5-MeO-DMT formed one hydrogen bond with the active site residue of 5HT2AR, where the nitrogen atom present at the 1st position of indole ring created a hydrogen bond with the backbone OH of Ser242 (NH···OH-; 2.24Å), furthermore electrostatic interaction exhibited between positively charged nitrogen ion attached to 3rd position of indole ring via ethyl side chain and negatively charged oxygen atom present in the backbone of Asp155 (N+···O- -; 2.75Å) Both indole rings (benzene and pyrrole) showed pi-pi interactions with Phe340 (5.27Å and 4.74Å). Few hydrophobic interactions Phe340, Phe339, Trp336, Leu229, Ile152, Val156, Phe234, Val235, Tyr370 and Val366 stabilized the Complex.

Another hit compound, 7-MeO-DMT, had equivalent pi-pi stacking with Phe340 at a distance of 4.86Å and 5.49Å and similar electrostatic interaction as that of 5-MeO-DMT along with few hydrophobic interactions Phe340, Phe339, Trp336, Leu229, Ile152, Val156, Phe234, Val235, Tyr370 and Val366 which stabilized the complex. Post-docking minimization revealed binding free energies (ΔBind) of 5-MeO-DMT and 7-MeO-DMT as -51.68 and -73.25 kcal/mol respectively. As shown in table 2, the significant Coulombic energy of -18.61 and -48.73 kcal/mol, while the somewhat preferred hydrophobic energy terms (ΔLipo) of -13.76 and -3.82 kcal/mol favor total binding energy.

3.2. ADME Study

The in-silico ADME characteristics of 5-MeO-DMT and 7-MeO-DMT are tabulated in Table 3. When both compounds were studied for Lipinski's rule of five, it was observed that they both do not violate any parameters. Both compounds showed a better- predicted gut permeability as QPPCaco values are >1160. Since, logBB is 0.42 so both 5-MeO-DMT and 7-MeO-DMT can cross BBB. The number of potential metabolic reactions is displayed by #metab lies in the normal range.

Table 3. The ADME properties of 5-MeO-DMT and 6-MeO-DMT with the normal range of each property

Compound	MW	CNS	HBD	HBA	QPlogPo/w	QPPCaco	QPlogBB	#metab	% Human Oral absorption	Rule of Five
5-MeO-DMT	218.298	1	1	2.75	2.64	1164.41	0.42	3	100.00	0
7-MeO-DMT	218.298	1	1	2.75	2.65	1172.58	0.42	4	100.00	0
Limits	130.0 to 725.0	–2 inactive +2 (active)	0.0 to 6.0	2.0 to 20.0	–2.0 to 6.5	<25 poor >500 great	–3.0 to 1.2	1-8	>80% is high <25% is poor	Max 4

3.3. Molecular dynamic simulation

100 ns molecular dynamic simulation of the bound 5-MeO-DMT/6WGT complex demonstrated that the RMSD of protein Cα atoms (Figure 5a) was stabilized following ligand binding, with modest oscillation ranging from 3.0 to 5.3Å after the first 20ns. The ligand RMSD fluctuated greatly over the first 20ns, ranging from 2.2 to 4.4Å, before stabilizing at 3.8 to 5.1Å until 100 ns. The flexibility of residues on ligand binding is investigated using root mean square fluctuations

(RMSFs) metrics. Highest of flexibility were observed with RMSF of Asp1045 (Cα: 9.56Å, Backbone: 9.22Å) and Ser1055 (Cα: 7.47Å, Backbone: 7.10Å) whereas low RMSF was reported for residues Asp155 (Cα: 0.65Å, Backbone: 0.67Å) and Ser159 (Cα: 0.65Å, Backbone: 0.70Å) (Figure 6a).

Hydrogen bonds, hydrophobic bonds, ionic interactions, and water bridges with Leu123, Ser131, Trp151, Ile152, Asp155, Val156, Ser159, Thr160, Cys227, Leu228, Leu229, Phe234, Val235, Ser242, Trp336, Phe339, Phe340, Asn343, Leu362, Val366 and Tyr370 helped place the molecule in the active pocket. From the ligand interaction fraction (Figure 7a) the nitrogen attached at third position of indole through ethyl side chain exhibited hydrogen bonding with Ser159 at 88% also exhibiting pi-cation interaction with Trp336 at 75%. Pyrrole ring of indole showing pi-pi stacking with Phe340 at 50% of total simulation trajectory (Figure 8a). Radius gyration, molecular surface area, solvent accessible surface area (SASA), and polar surface area (PSA) for ligands (Figure 9a) were all found to fall within the range of 3.00-3.47 Å, 236.03-249.11 $Å^2$, 0.269-47.56 $Å^2$ and 39.49-49.55 $Å^2$ respectively.

Another complex, 7-MeO-DMT/6WGT had its RMSD of protein Cα atoms calculated after a 100 nanoseconds molecular dynamic simulation of its docked postures and it exhibited a minor fluctuation of 1.5Å (3.0 to 4.5 Å) during first 45 nanoseconds. Furthermore, in the last 40 seconds, from 60 to 100ns, RMSD looks quite stable and fluctuated only in a range of 1.6 Å (4.0 to 5.6 Å) (Figure 5b).

The ligand RMSD showed the highest stability during the last 50 nanoseconds with the least fluctuation of 2Å. During the initial 50 nanoseconds studies, the RMSD of ligand was quite unstable exhibiting variations up to 5 Å (0.6 to 5.6 Å). The highest flexibility was observed with RMSF of Leu69 (Cα: 15.91 Å, backbone: 16.98 Å), His70 (Cα: 15.63 Å, backbone: 15.14 Å), and Leu71 (Cα: 14.41 Å, backbone: 13.76 Å), whereas low RMSF was reported for residues Asp115 (Cα: 0.77 Å, backbone: 0.78 Å), Val156 (Cα: 0.71 Å, backbone: 0.76 Å), Ser159 (Cα: 0.78 Å, backbone: 0.77 Å) and Phe340 (Cα: 0.76 Å, backbone: 0.80 Å) (Figure 6b).

The compound was mounted in the active pocket through ligand interaction (Figure 7b) forming hydrogen bonding (Asp115, Leu228, Leu229), hydrophobic interactions (Ile152, Val156, Ile206, Ile210, Phe234, Val235, Trp336, Phe339, The340, Val366), ionic & water bridged interaction (Asp155, Ser159, Ser242, Asn343). Using the results of 100 nanoseconds simulation study, a 2D ligand interaction diagram was created. The nitrogen present at the first position of the indole ring exhibited hydrogen bonding at 77% with Leu229, while the nitrogen attached to the third position of the indole ring via an ethyl side chain showed ionic interaction of 72 % with Asp155 & water bridged interaction of 24 % with Ser159 of the total simulation trajectory (Figure 8b).

Other ligand properties such as radius of gyration (3.00-3.60 Å), molecular surface area (230.91-247.87 $Å^2$), solvent accessible surface area (0.32-26.37 $Å^2$) and polar surface area (31.33-43.27 $Å^2$) were observed in these ranges respectively (Figure 9b).

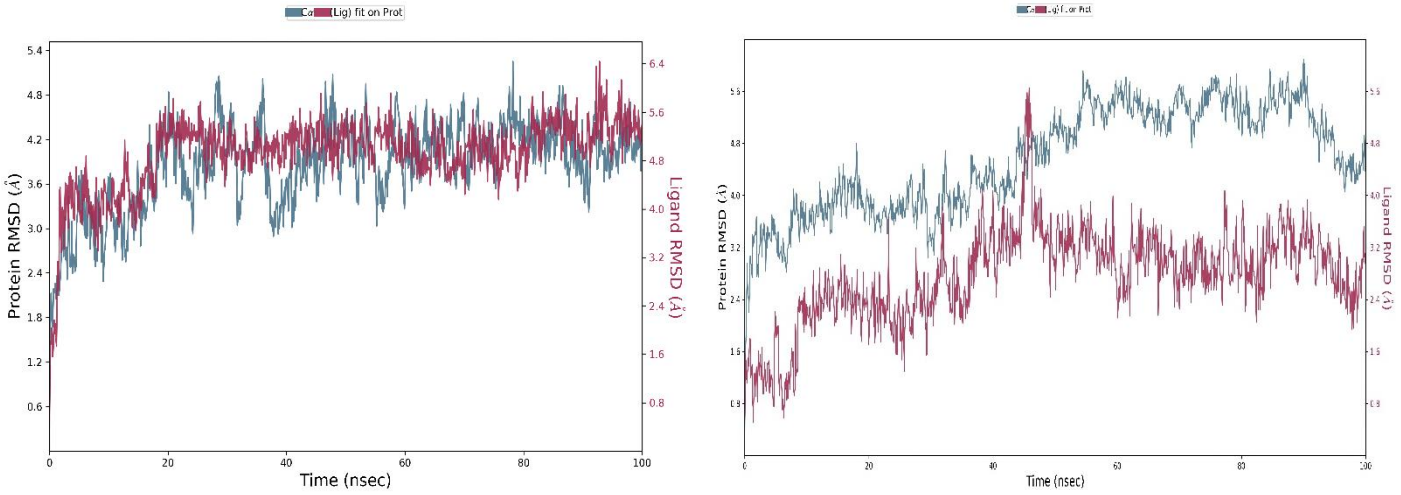

(a) **(b)**

Figure 5. RMSD plot illustrates the path of a 100ns simulation of **(a)** 5-MeO-DMT/6WGT complex; **(b)** 7-MeO-DMT/6WGT complex

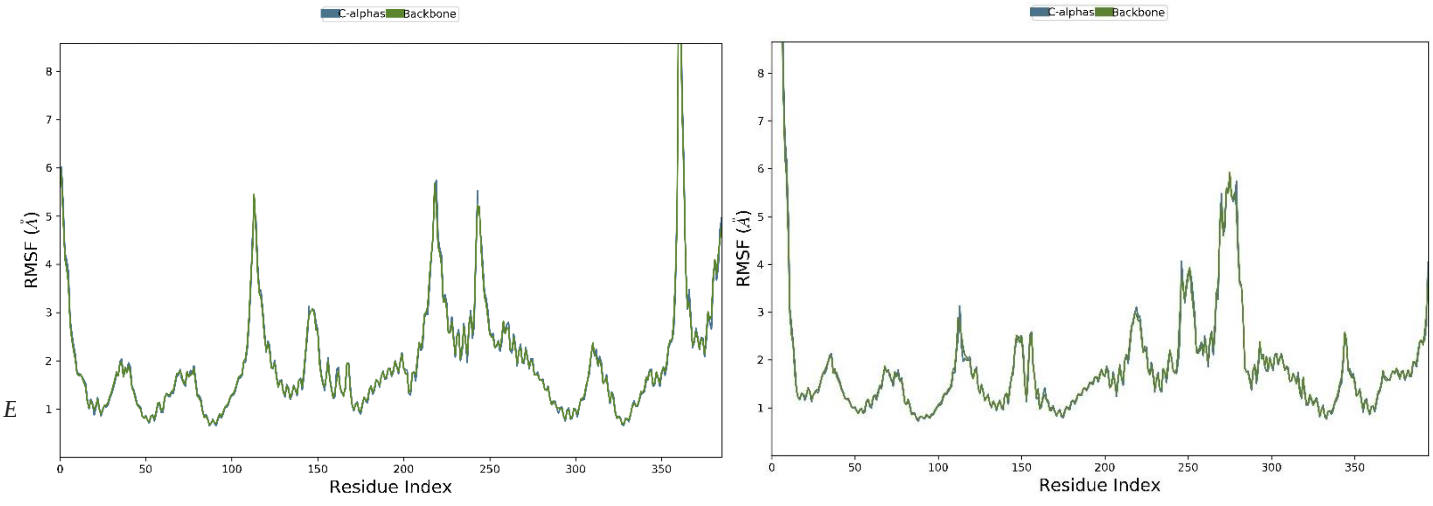

E

(a) **(b)**

Figure 6. RMSF plot illustrating the path of the 100ns simulation of **(a)** 5-MeO-DMT/6WGT complex; **(b)** 7-MeO-DMT/6WGT complex

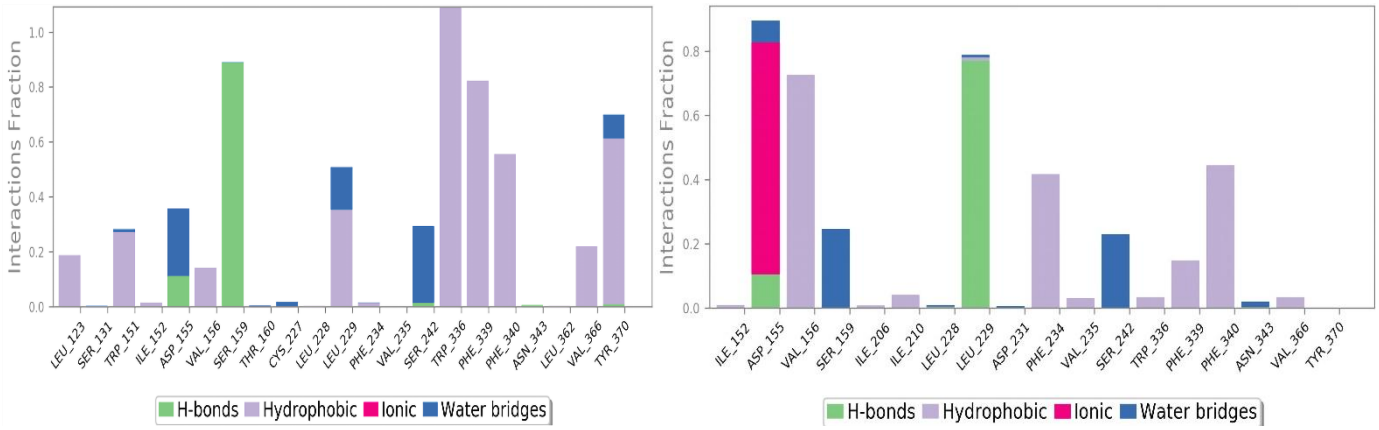

(a) **(b)**

Figure 7. The proportion of ligand interactions along the path of a 100ns simulation for **(a)** 5-MeO-DMT/6WGT complex; **(b)** 7-MeO-DMT/6WGT complex

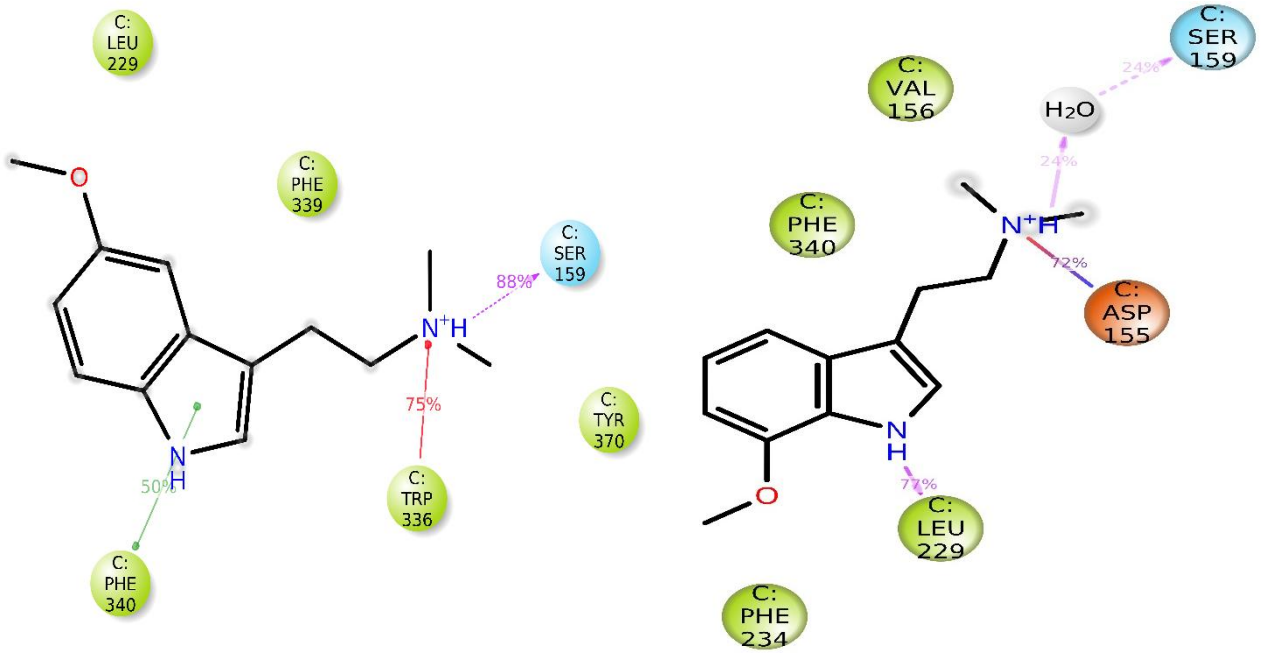

(a) **(b)**

Figure 8. 2D Interaction summary of **(a)** 5-MeO-DMT/6WGT complex **(b)** 7-MeO-DMT/6WGT complex

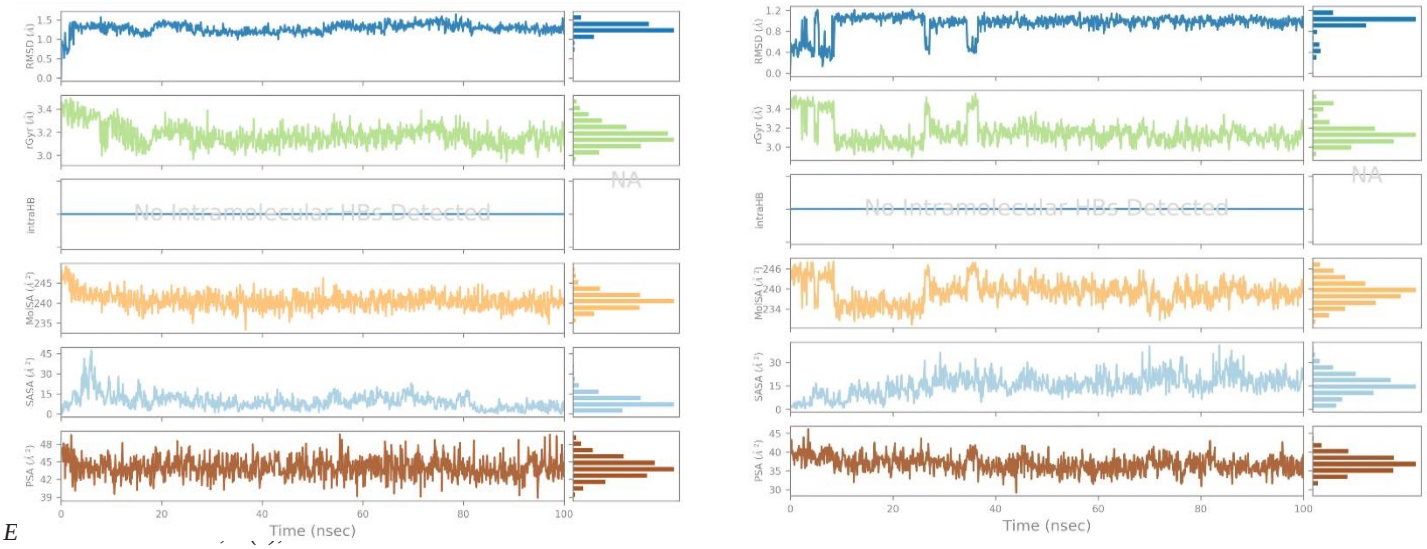

E

(a) **(b)**

Figure 9. Ligand properties for the 100ns simulation trajectory of **(a)** 5-MeO-DMT/6WGT complex **(b)** 7-MeO-DMT/6WGT complex

Conclusion

Persistent sensations of sorrow and disinterest are hallmarks of depression. Cognitive impairment, physical illness, and emotional and behavioral disorders are all possible outcomes. Those suffering from clinical depression often feel persistent sadness. The simple tasks of everyday life might feel insurmountable, and the sense that life is not worth fighting for can intensify. Researchers are motivated to produce effective antidepressants for the estimated 5% worldwide incidence of depression since depression is one of the most frequent mental health concerns.

Since 5-MeO-DMT has been shown to have antidepressant and anxiolytic properties, but also carries the hallucinogenic effects, 7-MeO-DMT, its non-hallucinogenic analogue, has undergone comparative in-silico studies against the 5HT2A receptor to validate whether or not it can be a potential candidate as an anti-depressant. Studies in ADME, molecular dynamic simulation, and binding free energy calculation have all been performed to verify a comparative molecular docking study.

According to the molecular docking studies, the Glide GScore for the compound 7-MeO-DMT is predicted to be -7.92 kcal/mol, when compared to the standard 5-MeO-DMT with the binding affinity of -8.01 kcal/mol it is more or less the equivalent furthermore in free energy calculation studies MM-GBSA (which reveals information about the free energy gap between the confined and completely unconstrained states) 7-MeO-DMT performed much better than that of 5-MeO-DMT where the scores are differentiated by 21.57 kcal/mol (7-MeO-DMT: -73.25 kcal/mol & 5-MeO-DMT: - 51.68 kcal/mol). In molecular dynamic simulation studies both 7-MeO-DMT and 5-MeO-DMT performed approximately the same. During RMSD calculation for backbone value ranges from 3.2 to 5.6 Å (7-MeO-DMT) and 3.0 to 5.4 Å (5-MeO-DMT) with a minor fluctuation of 2.4 Å over 100 ns simulation studies. The average root mean square fluctuation for C-alpha atoms of 7-MeO-DMT & 5-MeO-DMT noted to be 2.00 and 3.78 Å respectively. Radius gyration, molecular surface area, SASA, and PSA were likewise within the suitable range for ligand characteristics.

References

1. Fox ME, Lobo MK. The molecular and cellular mechanisms of depression: a focus on reward circuitry. Mol Psychiatry. 2019 Dec;24(12):1798–815.
2. Thase ME. A New Option for Depressed Patients Who Do Not Respond to Antidepressant Medications. AJP. 2023 Mar;180(3):188–9.
3. Proudman D, Greenberg P, Nellesen D. The Growing Burden of Major Depressive Disorders (MDD): Implications for Researchers and Policy Makers. Pharmacoeconomics. 2021;39(6):619–25.
4. Sachdeva P, Ji S, Ghosh S, Ghosh S, Raghunath M, Kim H, et al. Plausible Role of Stem Cell Types for Treating and Understanding the Pathophysiology of Depression. Pharmaceutics. 2023 Mar;15(3):814.
5. Constable PA, Al-Dasooqi D, Bruce R, Prem-Senthil M. A Review of Ocular Complications Associated with Medications Used for Anxiety, Depression, and Stress. Clin Optom (Auckl). 2022;14:13–25.
6. Moncrieff J, Cooper RE, Stockmann T, Amendola S, Hengartner MP, Horowitz MA. The serotonin theory of depression: a systematic umbrella review of the evidence. Mol Psychiatry. 2022 Jul 20;1–14.
7. Hasler G. Pathophysiology of depression: do we have any solid evidence of interest to clinicians? World Psychiatry. 2010 Oct;9(3):155–61.
8. Kwan AC, Olson DE, Preller KH, Roth BL. The neural basis of psychedelic action. Nat Neurosci. 2022 Nov;25(11):1407–19.
9. Vargas MV, Meyer R, Avanes AA, Rus M, Olson DE. Psychedelics and Other Psychoplastogens for Treating Mental Illness. Frontiers in Psychiatry [Internet]. 2021 [cited 2023 Apr 6];12. Available from: https://www.frontiersin.org/articles/10.3389/fpsyt.2021.727117
10. Davis AK, So S, Lancelotta R, Barsuglia JP, Griffiths RR. 5-methoxy-N,N-dimethyltryptamine (5-MeO-DMT) used in a naturalistic group setting is associated with unintended improvements in depression and anxiety. Am J Drug Alcohol Abuse. 2019;45(2):161–9.
11. Gable RS. Risk assessment of ritual use of oral dimethyltryptamine (DMT) and harmala alkaloids. Addiction. 2007 Jan;102(1):24–34.
12. Ermakova AO, Dunbar F, Rucker J, Johnson MW. A narrative synthesis of research with 5-MeO-DMT. J Psychopharmacol. 2022 Mar;36(3):273–94.
13. Delgado PL. Depression: the case for a monoamine deficiency. J Clin Psychiatry. 2000;61 Suppl 6:7–11.
14. Weil AT, Davis W. Bufo alvarius: a potent hallucinogen of animal origin. J Ethnopharmacol. 1994 Jan;41(1–2):1–8.
15. Lowe H, Toyang N, Steele B, Grant J, Ali A, Gordon L, et al. Psychedelics: Alternative and Potential Therapeutic Options for Treating Mood and Anxiety Disorders. Molecules. 2022 Apr 14;27(8):2520.
16. Jiang XL, Shen HW, Mager DE, Yu AM. Pharmacokinetic interactions between monoamine oxidase A inhibitor harmaline and 5-methoxy-N,N-dimethyltryptamine, and the impact of CYP2D6 status. Drug Metab Dispos. 2013 May;41(5):975–86.
17. Williams DA, Lemke TL. Foye's principles of medicinal chemistry [Internet]. 5th ed. Philadelphia: Lippincott Williams & Wilkins; 2002 [cited 2023 May 20]. 1114 p. Available from: http://catdir.loc.gov/catdir/enhancements/fy0711/2001050327-d.html
18. McClure-Begley TD, Roth BL. The promises and perils of psychedelic pharmacology for psychiatry. Nat Rev Drug Discov. 2022 Jun;21(6):463–73.
19. Cameron LP, Tombari RJ, Lu J, Pell AJ, Hurley ZQ, Ehinger Y, et al. A non-hallucinogenic psychedelic analogue with therapeutic potential. Nature. 2021 Jan;589(7842):474–9.
20. Zhang G, Stackman RW. The role of serotonin 5-HT2A receptors in memory and cognition. Front Pharmacol. 2015 Oct 6;6:225.
21. Dong C, Ly C, Dunlap LE, Vargas MV, Sun J, Hwang IW, et al. Psychedelic-inspired drug discovery using an engineered biosensor. Cell. 2021 May 13;184(10):2779-2792.e18.
22. Zięba A, Stępnicki P, Matosiuk D, Kaczor AA. Overcoming Depression with 5-HT2A Receptor Ligands. Int J Mol Sci. 2021 Dec 21;23(1):10.
23. Cameron LP, Olson DE. Dark Classics in Chemical Neuroscience: N, N-Dimethyltryptamine (DMT). ACS Chem Neurosci. 2018 Oct 17;9(10):2344–57.
24. Craske MG, Herzallah MM, Nusslock R, Patel V. From neural circuits to communities: an integrative multidisciplinary roadmap for global mental health. Nat Mental Health. 2023 Jan;1(1):12–

24.

25. Kim K, Che T, Panova O, DiBerto JF, Lyu J, Krumm BE, et al. Structure of a Hallucinogen-Activated Gq-Coupled 5-HT2A Serotonin Receptor. Cell. 2020 Sep 17;182(6):1574-1588.e19.

26. Greenwood JR, Calkins D, Sullivan AP, Shelley JC. Towards the comprehensive, rapid, and accurate prediction of the favorable tautomeric states of drug-like molecules in aqueous solution. J Comput Aided Mol Des. 2010 Jun;24(6–7):591–604.

27. Shelley JC, Cholleti A, Frye LL, Greenwood JR, Timlin MR, Uchimaya M. Epik: a software program for pK(a) prediction and protonation state generation for drug-like molecules. J Comput Aided Mol Des. 2007 Dec;21(12):681–91.

28. Harder E, Damm W, Maple J, Wu C, Reboul M, Xiang JY, et al. OPLS3: A Force Field Providing Broad Coverage of Drug-like Small Molecules and Proteins. J Chem Theory Comput. 2016 Jan 12;12(1):281–96.

29. Cherinka B, Andrews BH, Sánchez-Gallego J, Brownstein J, Argudo-Fernández M, Blanton M, et al. Marvin: A Tool Kit for Streamlined Access and Visualization of the SDSS-IV MaNGA Data Set. AJ. 2019 Jul;158(2):74.

30. McConkey BJ, Sobolev V, Edelman M. The performance of current methods in ligand–protein docking. Current Science. 2002;83(7):845–56.

31. Schrödinger Release 2023-1: QikProp, Schrödinger, LLC, New York, NY, 2021. [Internet]. [cited 2023 Mar 4]. Available from: https://www.google.com/search?q=Schr%C3%B6dinger+Release+2023-1%3A+QikProp%2C+Schr%C3%B6dinger%2C+LLC%2C+New+York%2C+NY%2C+2021.&newwindow=1&rlz=1C1CHBF_enIN1009IN1009&sxsrf=AJOqlzUZf-lQhrOPif2TBQSq5UN7UzrnAA%3A1677946647875&ei=F28DZNCINfrw4-EP_KeMmAo&ved=0ahUKEwiQ8Jev1sL9AhV6-DgGHfwTA6MQ4dUDCA8&oq=Schr%C3%B6dinger+Release+2023-1%3A+QikProp%2C+Schr%C3%B6dinger%2C+LLC%2C+New+York%2C+NY%2C+2021.&gs_lcp=Cgxnd3Mtd2l6LXNlcnAQDDoKCAAQRxDWBBCwA0oECEEYAFCICViICWCKrAJoAXABeACAAYsCiAGLApIBAzItMZgBAKABAcgBCMABAQ&sclient=gws-wiz-serp

32. Jacobson MP, Pincus DL, Rapp CS, Day TJF, Honig B, Shaw DE, et al. A hierarchical approach to all-atom protein loop prediction. Proteins: Structure, Function, and Bioinformatics. 2004;55(2):351–67.

33. Bowers K, Chow E, Xu H, Dror R, Eastwood M, Gregersen B, et al. Scalable Algorithms for Molecular Dynamics Simulations on Commodity Clusters [Internet]. ACM/IEEE SC 2006 Conference (SC'06). [cited 2023 Mar 4]. Available from: https://www.infona.pl//resource/bwmeta1.element.ieee-art-000004090217

34. Sidler D, Riniker S. Fast Nosé–Hoover thermostat: molecular dynamics in quasi-thermodynamic equilibrium. Phys Chem Chem Phys. 2019 Mar 13;21(11):6059–70.

35. Lippert RA, Predescu C, Ierardi DJ, Mackenzie KM, Eastwood MP, Dror RO, et al. Accurate and efficient integration for molecular dynamics simulations at constant temperature and pressure. J Chem Phys. 2013 Oct 28;139(16):164106.